Circular dichroism in laser-assisted proton-hydrogen collisions

Thomas Niederhausen*
James R. MacDonald Laboratory, Kansas State University, Manhattan, Kansas 66506-2604, USA

Bernold Feuerstein†
Max-Planck-Institut für Kernphysik, Heidelberg, Germany

Uwe Thumm‡
James R. MacDonald Laboratory, Kansas State University, Manhattan, Kansas 66506-2604, USA
(Received 20 April 2004; published 19 August 2004)

We investigate the effects of a strong laser field on the dynamics of electron capture and emission in ion-atom collisions within a reduced dimensionality model of the scattering system in which the motion of the active electron and the laser electric field vector are confined to the scattering plane. We examine the probabilities for electron capture and ionization as a function of the laser intensity, the projectile impact parameter b, and the laser phase ϕ that determines the orientation of the laser electric field with respect to the internuclear axis at the time of closest approach between target and projectile. Our results for the b-dependent ionization and capture probabilities show a strong dependence on both ϕ and the helicity of the circularly polarized laser light. For intensities above 5×10^{12} W/cm^2 our model predicts a noticeable circular dichroism in the capture probability for slow proton-hydrogen collisions, which persists after averaging over ϕ. Capture and electron emission probabilities defer significantly from results for laser-unassisted collisions. Furthermore, we find evidence for a charge-resonance-enhanced ionization mechanism that may enable the measurement of the absolute laser phase ϕ.

DOI: 10.1103/PhysRevA.70.023408 PACS number(s): 34.50.Rk, 34.70.+e, 32.80.Qk

I. INTRODUCTION

The study of charge exchange in ion-atom collisions dates back to the beginning of the last century, when Henderson [1] experimentally discovered electron capture by α particles passing through matter and was pursued actively over many decades [2]. More recently, the COLTRIMS technique [3,4] has allowed for the investigation of the electron dynamics in ion-atom collisions with unprecedented resolution in energy and momentum of the interacting electrons and nuclei. Independently, the interaction of strong laser fields with atoms, ions, or molecules has been addressed in a large number of experimental and theoretical investigations [5,6] over the past two decades. Even though the detailed investigation of laser-assisted heavy-particle collisions may ultimately help in steering chemical reactions into specific reaction channels by adjusting laser parameters (intensity, wavelength, and pulse shape), the promising combination of the two research areas—laser-matter interactions and heavy-particle collisions—has been the subject of only a few experiments with crossed heavy-particle and laser beams. For example, Débarre and Cahuzac [7] observed laser-induced charge exchange between Sr^+ and Ba in a mixture of strontium and barium vapors using Nd-YAG lasers with relatively very low intensities up to 5×10^8 W/cm^2. Grosser *et al.* [8] used a continuous beam of Na atoms, a pulsed beam of Kr atoms, and two pulsed (pump and probe) laser beams and crossed all beams in a small interaction volume. They explained an oscillatory structure in the angular distribution of excited Na projectiles after laser-assisted collisions with Kr atoms in terms of optical molecular transitions in the transient NaKr complex.

So far, technical challenges in the generation of sufficiently long and intense laser pulses and the synchronization of laser pulses within the interaction time interval (typically not more than 10^{-13} s in slow ion-atom collisions) have prevented a more detailed experimental investigation of laser-assisted or laser-controlled charge-exchange reactions in heavy-particle collisions. With the increasing availability of energetic lasers in atomic collision laboratories [4,9], we expect laser-induced effects in laser-assisted heavy-particle collisions to become observable. High laser intensities, focused on relatively large areas and long laser pulse durations, will significantly improve the statistics in laser-assisted collision experiments and are expected to soon open the door towards more detailed experimental studies that may contribute substantially to our understanding of laser-controlled chemical reactions.

On the theoretical side, a variety of methods have been applied to the calculation of charge exchange and electron emission in laser-assisted heavy-particle collisions. Li *et al.* [10,11] predicted, within lowest-order perturbation theory in the electron nucleus interaction, that the dressing of atomic levels in an intense laser field leads to a significant modification of capture and ionization cross sections in fast proton-hydrogen collisions. Voitkiv and Ullrich [12] found, also within lowest-order perturbation theory in the electron-projectile interaction, that a linearly polarized laser field can

*Electronic address: esdimax@phys.ksu.edu
†Electronic address: Bernold.Feuerstein@mpi-hd.mpg.de
‡Electronic address: thumm@phys.ksu.edu

substantially influence the binary-encounter electron emission process in fast collisions of α particles with hydrogen atoms. Close-coupling calculations for heavy-particle collisions, taking place in a strong laser pulse, were recently performed by Madsen *et al.* [13] and Kirchner [14]. Madsen *et al.* predicted a strong laser-induced modification of the *s-p* excitation probability in laser-assisted proton-H(1*s*) and proton-Na(3*s*) collisions. Kirchner found a strong influence of the electron capture and loss probabilities in laser-assisted He^{2+}-H collisions on the laser wavelength and the initial phase of the laser electric field. Lattice calculations on a three-dimensional Cartesian grid for laser-assisted proton collisions with lithium atoms in ground and excited states by Pindzola *et al.* [15] show a significant modification of the charge-transfer process for moderate laser intensities of 10^{12} W/cm^2. Lein and Rost [16] applied a reduced dimensionality model, solved the Schrödinger equation on a two-dimensional Cartesian grid, and predicted the generation of ultrahigh harmonics in laser-assisted collisions of 2 keV protons with hydrogen atoms in linearly polarized laser pulses with 16 optical cycles, a wavelength of 800 nm, and 10^{14} W/cm^2 intensity.

More work, both experimental and theoretical, has been done for laser-assisted electron scattering, but even a structureless projectile constitutes a serious challenge to present theories [17–19]. The early theory of Kroll and Watson [20] which only retained terms to first order in the photon frequency disagrees with the experimental results of Wallbank and Holmes [21]. This discrepancy between theory and experiment was traced to off-shell effects in the long-range polarization part of the electron-atom scattering potential [22]. Joachain, Dörr, and Kylstra [18] introduced the nonperturbative *R*-matrix Floquet method which was subsequently applied to multiphoton ionization, higher-harmonic generation, and laser-assisted electron atom collisions. Electron-ion collisions have recently attracted considerable interest as an integral part of the rescattering process, in which nonsequential double ionization of an atom or molecule is explained in terms of electron impact ionization of one electron by the laser-driven and rescattered other electron [9,23].

To the best of our knowledge, laser-assisted ion-atom collisions in circularly polarized light have not yet been investigated. In this paper we numerically solve the Schrödinger equation on a two-dimensional grid. Within this reduced dimensionality model, the electronic motion and the rotating laser electric field are confined to the scattering plane. For projectiles (protons) on a classical straight-line trajectory, we study the dependence of the probabilities for electron loss, capture, and emission on the intensity and helicity of the laser electric field. Even though experimental results are expected to differ slightly from the predictions of our two-dimensional calculations, we expect our results to be of sufficient accuracy to provide useful estimates for optimized laser and collision parameters that most clearly display the effects of a laser pulse on the electronic dynamics in heavy-particle collisions. Our numerical results show the strongest influence of the laser electric field on the capture probability at a laser intensity of 0.0014 a.u. (5.0×10^{13} W/cm^2)—i.e., when the laser electric force equals a few percent of the electrostatic Coulomb force exerted on the active electron by the target nucleus.

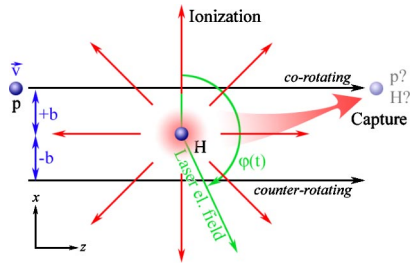

FIG. 1. (Color online) Collision scenario for a proton on a straight-line trajectory with impact parameter b and velocity v colliding with an atomic hydrogen target. The rotating laser electric field breaks the azimuthal symmetry: For positive impact parameters, the projectile follows the rotating laser field (corotating case); for negative impact parameters, the projectile moves against the rotating electric field (counterrotating case).

II. THEORY

A. Potentials

Unless indicated otherwise we will use atomic units ($\hbar = m_e = e = 1$) throughout this paper. For the impact energies considered in this work, we may neglect the nucleus-nucleus interaction and assume that the projectile ion of mass m_P moves along a straight-line trajectory in the z direction,

$$\vec{R}(t) = b\vec{e}_x + v(t - t_0)\vec{e}_z, \tag{1}$$

which is characterized by the impact parameter b, the constant velocity v, and the time of closest approach t_0 (Fig. 1).

Taking the location of the target as the coordinate origin, we employ two-dimensional soft-core Coulomb potentials

$$V_T^{e^-} = -\frac{1}{\sqrt{x^2 + z^2 + a}} \tag{2}$$

and

$$V_P^{e^-}(t) = -\frac{1}{\sqrt{(x-b)^2 + [z - v(t - t_0)]^2 + a}} \tag{3}$$

to represent the electronic interaction with the target and projectile nucleus, respectively. The "softening" parameter $a = 0.641$ regularizes the potentials at the location of the nuclei and is adjusted to reproduce the ground-state binding energy of atomic hydrogen.

In the dipole approximation, the interaction between the active electron and a monochromatic laser electric field of angular frequency ω,

$$E_x(t) = E_0(t)\cos[\omega(t - t_0) + \phi], \tag{4}$$

$$E_z(t) = E_0(t)\epsilon \sin[\omega(t - t_0) + \phi], \tag{5}$$

is given by the potential

$$V_L(x,z,t) = E_x(t)x + E_z(t)z \tag{6}$$

(Figs. 1 and 2). Here $\epsilon \in [-1,1]$ denotes the ellipticity of the laser light. The laser phase ϕ determines the direction of the laser electric field at the time of closest approach $t = t_0$ between the projectile and target.

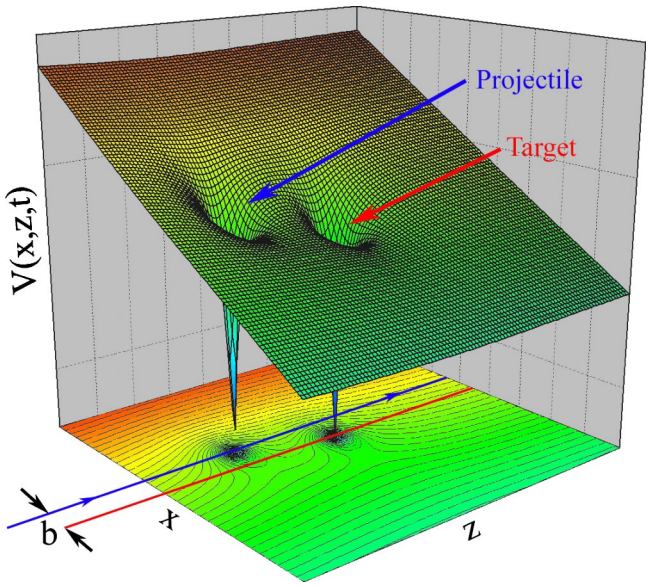

FIG. 2. (Color online) Snapshot of the electronic potential. For negative helicity, the laser electric field causes a clockwise rotation of the inclined potential plane about the target while the projectile moves toward the right-rear end along a straight line.

For the numerical applications in this work, we assume circularly polarized light of positive helicity ($\epsilon=1$), corresponding to clockwise rotation of the laser electric field vector in the zx plane (Fig. 1). The wave vector of the incident laser light is directed into the collision plane in Fig. 1. The envelope function $E_0(t)$ of the laser electric field turns the laser smoothly on during the time τ and then remains constant, once it has reached the maximum field strength E_0:

$$E_0(t) = \begin{cases} E_0 \sin^2\left(\dfrac{\pi}{2}\dfrac{t}{\tau}\right), & 0 \leqslant t \leqslant \tau, \\ E_0 & t > \tau. \end{cases} \tag{7}$$

We assume $\tau \ll t_0$, such that the oscillating electric field is fully turned on before the collision. At the time of closest approach, the electric field is given by

$$E_x = E_0 \cos\phi, \quad E_z = E_0 \sin\phi. \tag{8}$$

The sign of the projectile angular momentum relative to the target center of mass, $\vec{L}=\vec{R}\times m_P\vec{v}$, depends on the sign of the impact parameter. $\vec{L}$ can be either parallel or antiparallel to the laser helicity vector. In the first case the projectile moves in the same direction around the target as the laser electric field. We will address this situation as *corotating* scenario. Similarly, for the *counterrotating* scenario $\vec{L}$ and the helicity vector are antiparallel.

The collision process in the laser field is symmetrical with respect to the simultaneous change in sign of helicity and impact parameter. We can therefore limit our calculations to a given helicity while allowing for both positive and negative impact parameters. In all calculations we will assume a clockwise rotating laser electric field (positive helicity—i.e., $\epsilon=1$). For the coordinate system given in Fig. 1 and for the laser light propagating into the plane of the figure co (counter) rotating collisions occur for positive (negative) impact parameters.

In order to suppress unphysical reflections of the electronic probability density at the boundaries of our rectangular numerical grid, we employ absorbing boundaries [24]. For example, for absorption beyond x_0 in the $+\vec{x}$ direction, this is achieved by adjusting the absorber strength s and absorber width x_a in the negative imaginary potential

$$V_A(x) = \begin{cases} -is\left(\dfrac{x-x_0}{x_0}\right)^2, & x_0 < x < x_0 + x_a, \\ 0, & \text{otherwise}, \end{cases} \tag{9}$$

so that the reflected probability flux becomes negligible. The net electronic potential to be used in wave function propagation is thus given

$$V(x,z,t) = V_T(x,z) + V_P(x,z,t) + V_L(x,z,t) + V_A(x,z), \tag{10}$$

where $V_A(x,z)$ models the absorption in all directions in obvious two-dimensional generalization of $V_A(x)$.

B. Dynamics

The solution of the time-dependent Schrödinger equation (TDSE) $i\partial_t|\Psi(t)\rangle = H(t)|\Psi(t)\rangle$ is formally given by the evolution of the initial wave function $\Psi(x,z,t=0)$,

$$\Psi(x,z,t) = \hat{T}\exp\left[-i\int_0^t dt' H(x,z,t')\right]\Psi(x,z,0), \tag{11}$$

with the time-ordering operator $\hat{T}$ and the Hamiltonian

$$H(t) = T_x + T_z + V(x,z,t). \tag{12}$$

T_x and T_z are the electronic kinetic energy operators. The numerical propagation of the TDSE (11) is carried out on a numerical grid using the unconditional stable Crank-Nicholson split-operator method [25,26]. For a time step Δt the wave function (11) at time $t+\Delta t$ is recursively given in terms of $\Psi(t)$ by

$$\Psi(t+\Delta t) \approx \exp\left[-iT_x\frac{\Delta t}{2}\right] \times \exp\{-i[T_z + V(x,z,t)]\Delta t\} \times \exp\left[-iT_x\frac{\Delta t}{2}\right]\Psi(t). \tag{13}$$

We choose equal grid spacings in x and z direction of $\Delta x = \Delta z = 0.2$. Our grid covers 120 a.u. along the projectile trajectory (z direction) and has a variable length in the x direction, depending on the impact parameter, given by $80+|b|$. We implemented absorbing boundaries of widths $x_a = z_a = 20$ inside the grid boundaries with an absorption strength of $s = 0.01$. These absorber parameters produce converged results that do not differ from those obtained with altered absorbers of twice the absorption width or strength and show no signs of unphysical reflections at the grid edges.

The laser frequency was chosen in the near infrared with $\omega = 0.0428$, which corresponds to a wavelength of 1064 nm

available from common Nd:YAG lasers. After a initial ramping time $\tau=450=10.9$ fs we propagate the electronic wave function in the laser field for 550 a.u.=13.2 fs. A total propagation time in the laser field of $t_{max}=1450=35.1$ fs leads to converged results for capture and ionization probabilities for all relevant values of b and ϕ and for laser intensities between $2.85\times10^{-5}=1\times10^{12}$ W/cm^2 and $2.85\times10^{-3}=1\times10^{14}$ W/cm^2. Time steps of $\Delta t=0.1$ were found small enough to guarantee the long-term accuracy of the propagation scheme.

At each time step we integrate the probability density over two square boxes of length 20 a.u., centered on the projectile ion and target. For larger internuclear distances, we interpret these integrals $N_T(t)$ and $N_P(t)$ as as instantaneous electronic charge states on the projectile and target, respectively. At the end of the numerical propagation, at time $t=t_{max}$, they serve as approximations for the capture and ionization probabilities:

$$P^{\pm}_{cap}(b,\phi)=N_P(t=t_{max}), \tag{14}$$

$$P^{\pm}_{ion}(b,\phi)=[1-N_P(t=t_{max})-N_T(t=t_{max})]. \tag{15}$$

The superscripts $\pm$ distinguish between co $(+)$ and counter $(-)$ rotating collisions. Since the laser phase ϕ is currently not observable or experimentally controllable, we average over ϕ:

$$P^{\pm}_{cap}(b)=\frac{1}{2\pi}\int_0^{2\pi}d\phi P^{\pm}_{cap}(b,\phi), \tag{16}$$

$$P^{\pm}_{ion}(b)=\frac{1}{2\pi}\int_0^{2\pi}d\phi P^{\pm}_{ion}(b,\phi). \tag{17}$$

We found that it is sufficient to calculate the capture and ionization probability for eight different laser phases (between 0° and 315° with increments of 45°). Values for $P^{\pm}_{cap}(b,\phi)$ and $P^{\pm}_{ion}(b,\phi)$ at arbitrary values for ϕ are obtained by spline interpolation. Test calculations using 36 different phases with increments of 10° showed no relevant change in the interpolated probabilities.

Finally, we integrate over b in order to obtain total cross sections for capture and ionization:

$$\sigma^{\pm}_{cap}=2\pi\int_0^{\infty}dbbP^{\pm}_{cap}(b), \tag{18}$$

$$\sigma^{\pm}_{ion}=2\pi\int_0^{\infty}dbbP^{\pm}_{ion}(b). \tag{19}$$

We note that $P^{\pm}_{cap}(b,\phi)$ and $P^{\pm}_{ion}(b,\phi)$ are calculated within a two-dimensional model and that effects due to the reduced dimensionality are disregarded in the integration over b in $\sigma^{\pm}_{cap}$ and $\sigma^{\pm}_{ion}$.

III. NUMERICAL RESULTS

A. Field-free results

Reduced-dimensionality numerical capture probabilities for field-free proton-hydrogen collisions have been published by Lein and Rost [16]. Their results are almost identical with our field-free capture probabilities (Fig. 3). Total capture cross sections for collisions of 1–2 keV protons with atomic hydrogen have been measured by Gealy and Van Zyl [27]. For 2 keV incident kinetic energy, our calculated capture cross section is 44% larger than the experimental value. For 1 keV protons it is 34% larger (Table I).

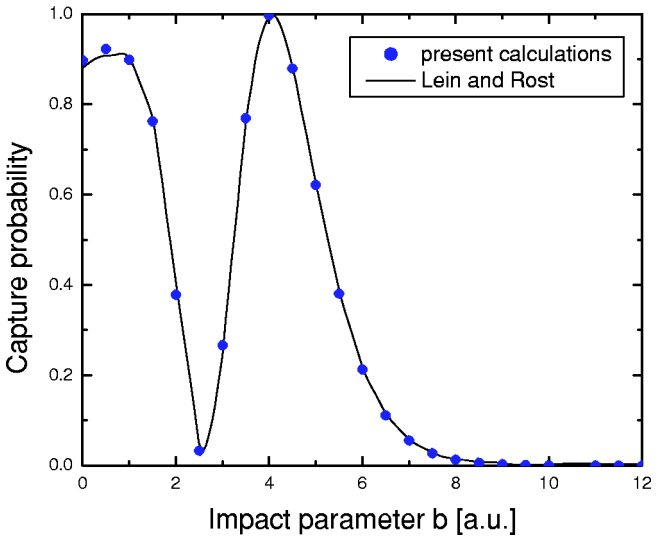

FIG. 3. (Color online) Capture probability as a function of the impact parameter for field-free collisions of 2 keV protons with hydrogen atoms. Results from independent two-dimensional wave function propagation calculations: Lein and Rost [16] (solid curve), present results (dots).

The difference between the measured and calculated cross sections can be understood in terms of a simple overlap argument. Compared to experiment or full-dimensionality calculations, the smaller phase space inherent in reduced-dimensionality calculations increases the wave function overlap between the interacting projectile and target, thus resulting in larger calculated cross sections (Table I). However, we do not expect that the main conclusions from our numerical results for laser-assisted collisions (see below) are significantly influenced by reducing the dimensionality from 3 to 2. In particular, reduced-dimensionality results that indicate a strong relative difference in the capture or ionization cross sections between corotating and counterrotating laser-assisted collisions are expected to be observable.

B. Circular polarization

The presence of the laser radiation during the collision process results in an additional dependence of the electronic

TABLE I. Comparison of the calculated (reduced dimensionality) total capture cross sections for field-free collisions with the experiment of Gealy and Van Zyl [27].

	Electron capture cross section		
Energy (keV)	σ^{theor}_{cap} (10^{-16} cm^2)	σ^{expt}_{cap} (10^{-16} cm^2)	Difference
1	21.87	16.3±18%	34%
2	20.04	13.9±17%	44%

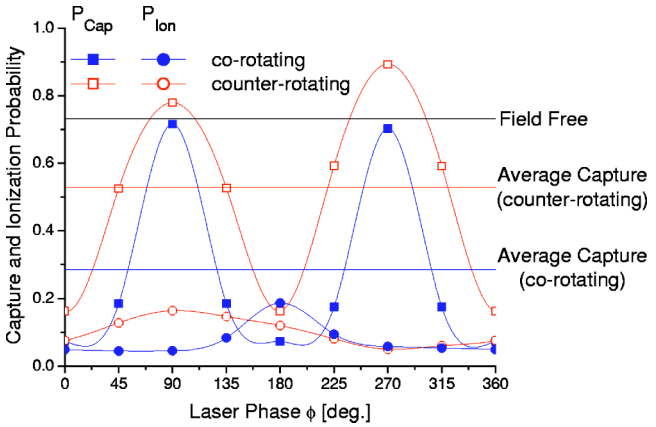

FIG. 4. (Color online) Capture and ionization probability as a function of the laser phase ϕ at the time of closest approach between projectile and target for 1.21-keV p-H collisions. The impact parameter is $b=\pm 4$ a.u. and the laser intensity 5×10^{13} W/cm^2. Phase-averaged results for the capture probability differ significantly for corotating and counterrotating laser-assisted collisions.

dynamics on the laser phase ϕ at the time of closest approach. Our results for a fixed impact parameter $b=\pm 4$ and laser intensity 5×10^{13} W/cm^2 for the capture probability as a function of ϕ show large amplitude oscillations and differ from the field-free results most strikingly for $\phi=0°$ and 180° (Fig. 4). They also display a strong dichroism effect—i.e., a substantial difference in the electron capture probability for positive and negative impact parameters or, equivalently, for corotating as compared to counterrotating collisions.

In comparison to the phase-averaged results for the field-free case, we find that the capture probabilities in both corotating and counterrotating collisions are considerably reduced. The ionization probabilities depend less sensitively on ϕ, and their phase averages (not shown in Fig. 4) differ much less for corotating and counterrotating collisions (positive and negative impact parameters) than the phase-averaged capture probabilities. This tendency of weak dichroism in the ionization probability extends to other impact parameters, as will be discussed below. In the following discussion, we will first focus on the strong dichroism apparent in the capture probability, followed by an analysis of the ionization process.

1. Electron capture

Figure 5(a), shows the electron capture probability as a function of the impact parameter and the laser phase ϕ for a laser intensity of $I=5\times 10^{13}$ W/cm^2. The electron capture probability shows maxima at impact parameters $b=\pm 2$ and $b\approx\pm 4.0$. Similar structures appear for the field-free capture probability (Fig. 3). They originate in the large wave function overlap of the corresponding target and projectile states near the point of closest approach.

With regard to the dependence on the phase of the rotating laser field, the capture probability shows a strong enhancement at $\phi=90°$ and 270°, when the force exerted by the laser electric field on the electron at the time t_0 of closest approach is either antiparallel or parallel to the direction of the projectile motion, respectively (see Fig. 1 and note that force and electric field point in opposite directions). For these particular phases, the field-modified Coulomb potentials of target and projectile are identical at t_0, and the internuclear axis is momentarily perpendicular to the laser electric field. This implies perfect level matching of field-dressed projectile and target states and explains the large capture probabilities for $\phi=90°$ and 270° in Fig. 5(a).

To support this interpretation further, we also calculated the electron capture probability for a *constant* electric field, corresponding in direction and magnitude to the laser electric field at time t_0, with otherwise identical parameters [Fig. 5(d)]. In this calculation, ϕ parametrizes the direction of the stationary electric field. We note that this scenario is somewhat unrealistic, since a constant electric field would deflect the projectile ion and invalidate our assumption of a straight-line projectile trajectory. Interestingly, however, the dependence on the laser electric field direction of the capture probability in Fig. 5(d) compares well with the ϕ dependence in Fig. 5(a), thus adding credibility to the importance of energy-level matching between projectile and target states at time t_0.

For the laser phases $\phi=0°$ and 180° and positive impact parameters, the laser force on the electron at time t_0 points to the target or to the projectile, respectively (vice versa for negative impact parameters). The mismatch of the field-dressed hydrogen energy levels is largest at the time of closest approach, thus strongly suppressing electron capture in favor of enhanced ionization for $\phi=180°$ at positive impact parameters and for $\phi=0°$ at negative impact parameters [Fig. 5(b)].

Compared to the laser phase of 270°, Figs. 5(a) and 5(d) show a slightly reduced capture probability at $\phi=90°$, when the laser electric force on the electron at t_0 is antiparallel to the projectile velocity. The target electron loss probability [Figs. 5(c) and 5(d)] does not show this asymmetry, and the slightly larger capture probability for $\phi=270°$ appears to be due to the "extra push" the electron receives by the laser force at t_0 in direction of the projectile motion. In contrast, for $\phi=90°$, the electron is accelerated in the opposite direction by the laser force and is a little more likely to ionize.

Overall, Fig. 5(a) displays a strong enhancement of the electron capture probability for negative impact parameters (counterrotating collisions) in comparison with for positive impact parameters (corotating collisions), with much broader peaks at $\phi=90°$ and 270° for the counterrotating case.

If the laser electric field is oriented perpendicular to the internuclear axis, both Coulomb potentials are identical and electron transfer is most likely. For corotating collisions, the relative orientation of the laser electric field and internuclear axis changes much less rapidly during the collision time than for counterrotating collisions. At appropriate impact energies and impact parameters, this relative orientation is maintained throughout the projectile-target interaction for corotating collisions. During the interaction time, which is of the order of one laser cycle, the projectile and target will then form a short-lived quasimolecule. Thus, in conclusion, electron capture is expected to depend sensitively on the laser phase for corotating collisions.

In contrast, for counterrotating collisions, the angle between the rotating electric field of the laser light and the internuclear axis changes rapidly, irrespective of the value of

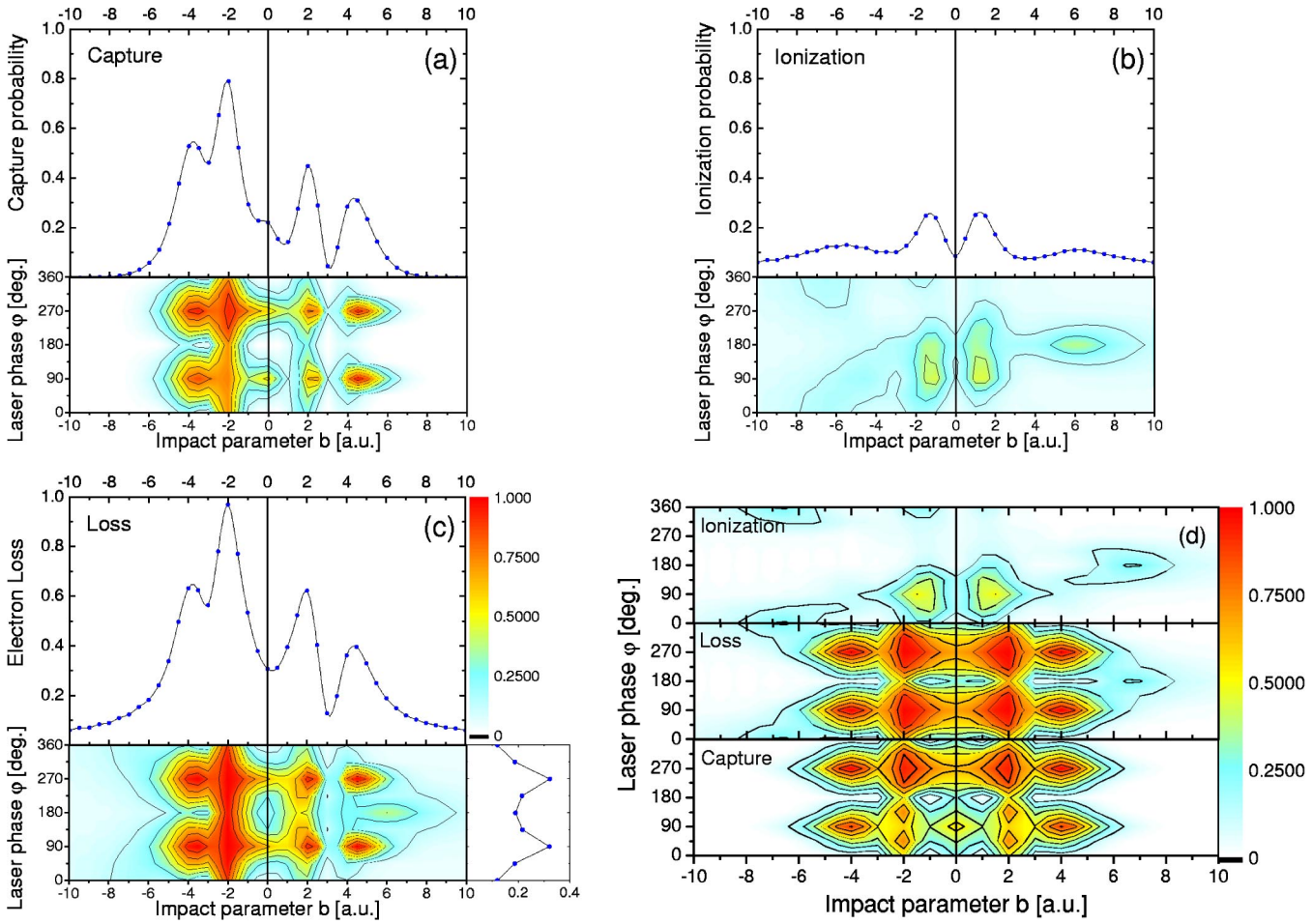

FIG. 5. (Color online) Electron capture (a), ionization (b), and target electron loss probability (c) in laser-assisted 1.21-keV p-H collisions for a laser intensity of $I=5\times10^{13}$ W/cm^2. The contour plots show the probabilities as a function of the impact parameter b and the laser phase ϕ. The probability difference between consecutive contour lines is 0.125. The top panels in (a), (b), and (c) show phase averaged results. The side panel in (c) shows the impact-parameter average as a function of the laser phase. Capture, ionization, and loss probabilities as a function of the impact parameter and the laser phase for the case of a *static* electric field, corresponding in the direction and magnitude to the laser electric field at the distance of closest approach in (a), (b), and (c), are shown in (d) for comparison.

ϕ. Level matching of projectile and target states occurs for a wide range of laser phases, but only for a small fraction of the interaction time. However, since the time scale of the electronic motion (1 a.u.) is about two orders of magnitude faster than a laser cycle (146.7 a.u.), the transient reflection symmetry of both Coulomb potentials still lasts long enough to enable noticeable electron transfer. In particular, at the chosen projectile velocity ($v=0.22$) electron transfer to the projectile is relatively likely, while recapture by the target is suppressed by the rapidly increasing asymmetry between the two laser-modified Coulomb potentials.

For the given projectile speed, this explains the enhancement of capture in counterrotating collisions. For corotating collisions, the relative orientation of the laser electric field and the internuclear axis is maintained for approximately half a laser cycle, and the formation of a transient molecule decreases the probability for the electron to remain in a projectile state. In agreement with this explanation, a numerical test has shown that the capture probability in corotating collisions is reduced, and the difference between corotating and counterrotating electron capture becomes much less pronounced projectiles if we double the impact velocity ($E_{kin}=4.83$ keV).

As mentioned earlier, the ϕ dependence in laser-assisted capture cross sections is difficult to resolve experimentally. Interestingly, however, the clear enhancement of the capture probability in counterrotating over corotating collisions remains after averaging over ϕ [top panel of Fig. 5(a)] and may be probed in angle-differential collision experiments, at appropriate projectile velocities.

2. Ionization

The ionization probabilities in Figs. 5(b) and 5(d) show a broad enhancement near $\phi=90°$ when the laser electric force on the electron opposes the projectile motion and for impact parameters around $b=\pm1.5$. A less pronounced enhancement in the ionization probability occurs at $b\sim\pm6$ [Fig. 5(b)].

For corotating collisions (positive b) and larger impact parameters, ionization is enhanced at a laser phase of 180°, while in the counterrotating case a much broader and weaker

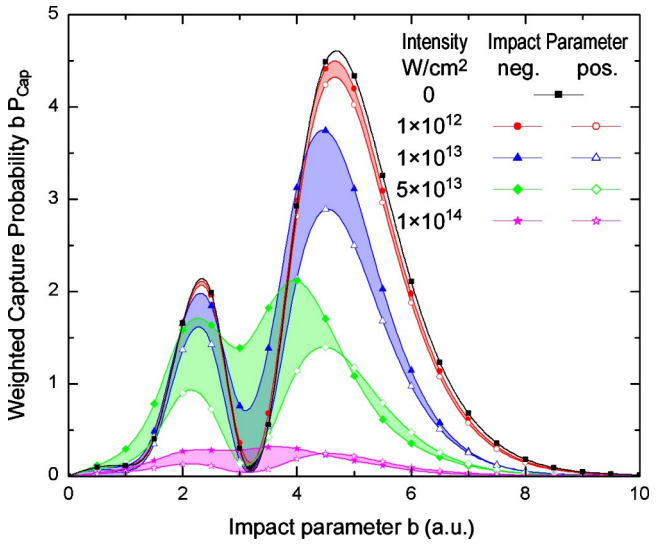

FIG. 6. (Color online) bP_{cap}, averaged over the laser phase, at different laser intensities for corotating (positive impact parameter) and counterrotating (negative impact parameters) collisions.

peek occurs near $\phi=0°$. In both cases the laser force on the electron points towards the projectile at the time of closest approach. This explains the signature of enhanced ionization in Fig. 5(b) at $\phi=0°$ and 180°. This enhancement corresponds to the well-known charge-resonance-enhanced ionization (CREI) during the fragmentation of diatomic molecules in strong laser fields at larger internuclear distances [28].

The broadening of the ionization peak for counterrotating collisions (negative b) is identical to the corresponding feature in the capture probability discussed earlier. In the corotating scenario, while near the target, the projectile moves along with the laser electric field vector. The Coulomb and laser electric forces then add to their maximal possible magnitude for a relatively long time. The time during which a maximal force is exerted on the electron is much smaller for the counterrotating case. Therefore, for counterrotating collisions, the CREI peak around $\phi=0°$ is weaker and less compressed than the CREI peak in corotating collisions at $\phi=180°$ [Fig. 5(b)]. The distinctive CREI peak might allow for the determination of the actual laser phase in future phase-locked experiments. Averaging over all laser phases ϕ removes the dichroism effect almost entirely [top panel in Fig. 5(b)].

3. Laser intensity dependence

Figure 6 shows the laser phase-averaged results for the weighted electron capture probability bP_{cap} at different laser intensities for corotating and counterrotating collisions. Noticeable differences between corotation and counterrotation appear above laser intensities of 5×10^{12} W/cm^2. The capture probability rapidly decreases for laser intensities above 1×10^{14} W/cm^2, when ionization begins to be the dominate. It is for all intensities smaller than for field-free collisions. The relative difference

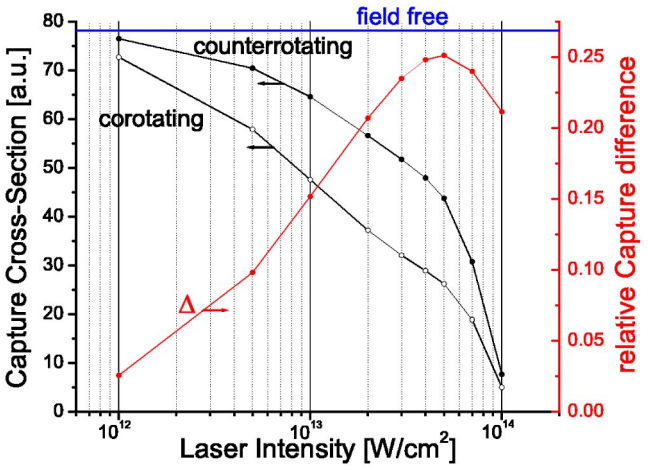

FIG. 7. (Color online) Total electron capture cross sections as a function of the laser intensity for corotating and counterrotating collisions. Also shown is the relative difference Δ, which is largest at a laser intensity of 5×10^{13} W/cm^2.

$$\Delta = \frac{|\sigma_{cap}^{+} - \sigma_{cap}^{-}|}{\sigma_{cap}^{+} + \sigma_{cap}^{-}|} \tag{20}$$

in the total electron capture cross section as a function of the laser intensity is shown in Fig. 7. The difference in the capture cross section or corotating and counterrotating collisions amounts to up to 40% at a laser intensity of 5×10^{13} W/cm^2 (Table II). We consider these differences as upper limits for the dichroism effect and expect them to decrease slightly in full three-dimensional calculations, since an added degree of freedom no longer limits the electronic motion to the plane in which the laser field rotates.

The results in Fig. 7 relate to *total* cross section only. Experimentally, *scattering-angle differential* cross sections [and $P(b)$] can be measured either directly by detecting the projectile scattering angle or indirectly by observing the recoil direction of the target. For scattering angles that correspond to impact parameters with the largest circular dichroism in $P(b)$, the dichroism effect is more pronounced in differential cross sections than in total cross sections (cf. Fig. 5).

TABLE II. Comparison of the total capture cross section for corotating and counterrotating collisions at different laser intensities.

Intensity (W/cm^2)	Electron capture cross section	
	Corotating	Counterrotating
0	78.08	78.08
1×10^{12}	72.67	76.47
5×10^{12}	57.85	70.41
1×10^{13}	47.53	64.52
5×10^{13}	26.18	43.74
1×10^{14}	4.97	7.63

IV. CONCLUSION

We have shown by numerically solving the Schrödinger equation within a two-dimensional model that a significant difference in the electron capture probabilities $P^{\pm}_{cap}(b)$ in corotating and counterrotating laser-assisted *p*-H collisions is due to a energy-level matching effect between the target and projectile states at relevant impact parameters. We thus predict a strong circular dichroism; i.e., we find that capture (and to a lesser extent ionization) probabilities are different for parallel and antiparallel laser helicity and projectile angular momentum.

Laser pulses with lengths of a few nanoseconds and intensities of about 5×10^{12} W/cm^2 and higher should allow for the experimental verification of the predicted dichroism in the capture probability. In addition, we found evidence for the charge-resonant-enhanced ionization mechanism in laser-assisted ionization. In conjunction with phase-locked lasers, this effect may be used in angle-differential laser-assisted collision experiments in order to select a specific orientation of the laser electric field at the time of closest approach between projectile and target.

We hope that this work will stimulate the challenging experimental test of the predicted effects, electron capture dichroism, and CREI in laser-assisted collisions. In the long run, this may lead to new and more efficient schemes for the control of chemical reactions with intense laser radiation.

ACKNOWLEDGMENTS

This work is supported by the NSF (Grant No. PHY-0071035) and the Division of Chemical Sciences, Office of Basic Energy Sciences, Office of Energy Research, U.S. DOE.

[1] G. H. Henderson, Proc. R. Soc. London, Ser. A **102**, 496 (1923).
[2] B. H. Bransden and M. R. C. McDowell, *Charge Exchange in the Theory of Ion-Atom Collisions* (Clarendon Press, Oxford, 1992).
[3] R. Dörner, V. Mergel, O. Jagutzki, L. Spielberger, J. Ullrich, R. Moshammer, and H. Schmidt-Böcking, Phys. Rep. **330**, 95 (2000).
[4] J. Ullrich, R. Moshammer, A. Dorn, R. Dörner, L. P. H. Schmidt, and H. Schmidt-Böcking, Rep. Prog. Phys. **66**, 1463 (2003).
[5] M. Protopapas, C. H. Keitel, and P. L. Knight, Rep. Prog. Phys. **60**, 389 (1997).
[6] B. Feuerstein and U. Thumm, Phys. Rev. A **67**, 043405 (2003).
[7] A. Débarre and P. Cahuzac, J. Phys. B **19**, 3965 (1986).
[8] J. Grosser, D. Hohmeiser, and S. Klose, J. Phys. B **29**, 299 (1996).
[9] A. S. Alnaser, T. Osipov, E. P. Benis, A. Wech, B. Shan, C. L. Cocke, X. M. Tong, and C. D. Lin, Phys. Rev. Lett. **91**, 163002 (2003).
[10] S.-M. Li, Y.-G. Miao, Z.-F. Zhou, J. Chen, and Y.-Y. Kiu, Z. Phys. D: At., Mol. Clusters **39**, 29 (1997).
[11] S.-M. Li, J. Chen, and Z.-F. Zhou, J. Phys. B **35**, 557 (2002).
[12] A. B. Voitkiv and J. Ullrich, J. Phys. B **34**, 1673 (2001).
[13] L. B. Madsen, J. P. Hansen, and L. Kocbach, Phys. Rev. Lett. **89**, 093202 (2002).
[14] T. Kirchner, Phys. Rev. Lett. **89**, 093203 (2002).
[15] M. S. Pindzola, T. Minami, and D. R. Schultz, Phys. Rev. A **68**, 013404 (2003).
[16] M. Lein and J. M. Rost, Phys. Rev. Lett. **91**, 243901 (2003).
[17] H. J. Mason, Rep. Prog. Phys. **56**, 1275 (1993).
[18] C. J. Joachain, M. Dörr, and N. Kylstra, Adv. At., Mol., Opt. Phys. **42**, 225 (2000).
[19] A. Cionga, F. Ehlotzky, and G. Zloh, J. Biol. Phys. **34**, 2057 (2001).
[20] N. M. Kroll and K. M. Watson, Phys. Rev. A **8**, 804 (1973).
[21] B. Wallbank and J. K. Holmes, J. Phys. B **27**, 1221 (1994); **27**, 5405 (1994).
[22] A. Jarón and J. Z. Kamiński, Phys. Rev. A **56**, R4393 (1997).
[23] R. Moshammer, B. Feuerstein, J. CrespoLopez-Urrutia, J. Deipenwisch, A. Dorn, D. Fischer, C. Höhr, P. Neumayer, C. D. Schröter, J. Ullrich, H. Rottke, C. Trump, M. Wittmann, G. Korn, and W. Sandner, Phys. Rev. A **65**, 035401 (2002).
[24] Himadri. S. Chakraborty, Thomas Niederhausen, and Uwe Thumm, Phys. Rev. A **69**, 052901 (2004).
[25] W. H. Press, B. P. Flannery, S. A. Teukolsky, and W. T. Vetterling, *Numerical Recipes in FORTRAN 77*, (Cambridge University Press, Cambridge, England, 1992), p. 842.
[26] U. Thumm, in *Book of Invited Papers, XXII ICPEAC, Santa Fe, NM*, edited by S. Datz *et al.* (Rinton Press, Princeton, NJ, 2002), p. 592.
[27] M. W. Gealy and B. Van Zyl, Phys. Rev. A **36**, 3091 (1987).
[28] A. D. Bandrauk and J. Ruel, Phys. Rev. A **59**, 2153 (1999).